

# Astronomical calibration of the Danian stage (Early Paleocene) revisited: Settling chronologies of sedimentary records across the Atlantic and Pacific Oceans

Jaume Dinarès-Turell <sup>a,\*</sup>, Thomas Westerhold <sup>b</sup>, Victoriano Pujalte <sup>c</sup>, Ursula Röhl <sup>b</sup>, Dick Kroon <sup>d</sup>

<sup>a</sup> Istituto Nazionale di Geofisica e Vulcanologia, Via di Vigna Murata 605, I-00143 Rome, Italy

<sup>b</sup> MARUM – Center for Marine Environmental Sciences, University of Bremen, Leobener Strasse, D-28359 Bremen, Germany

<sup>c</sup> Department of Stratigraphy and Paleontology, University of the Basque Country, UPV/EHU, PO Box 644, E-48080 Bilbao, Spain

<sup>d</sup> School of GeoSciences, Grant Institute, University of Edinburgh, King's Buildings, West Mains Road, Edinburgh, EH9 3JW, UK



## ARTICLE INFO

### Article history:

Received 13 May 2014

Received in revised form 2 August 2014

Accepted 23 August 2014

Available online 14 September 2014

Editor: J. Lynch-Stieglitz

### Keywords:

orbital tuning

magnetostratigraphy

cyclostratigraphy

Danian

ODP

## ABSTRACT

Astronomical tuning of sedimentary records to precise orbital solutions has led to unprecedented resolution in the geological time scale. However, the construction of a consistent astronomical time scale for the Paleocene is controversial due to uncertainties in the recognition of the exact number of 405-kyr eccentricity cycles and accurate correlation between key records. Here, we present a new Danian integrated stratigraphic framework using the land-based Zumaia and Sopelana hemipelagic sections from the Basque Basin and deep-sea records drilled during Ocean Drilling Program (ODP) Legs 198 (Shatsky Rise, North Pacific) and 208 (Walvis Ridge, South Atlantic) that solves previous discrepancies. The new coherent stratigraphy utilises composite images from ODP cores, a new whole-rock  $\delta^{13}\text{C}$  isotope record at Zumaia and new magnetostratigraphic data from Sopelana.

We consistently observe 11 405-kyr eccentricity cycles in all studied Danian successions. We achieve a robust correlation of bioevents and stable isotope events between all studied sections at the ~100-kyr short-eccentricity level, a prerequisite for paleoclimatic interpretations. Comparison with and subsequent tuning of the records to the latest orbital solution La2011 provides astronomically calibrated ages of  $66.022 \pm 0.040$  Ma and  $61.607 \pm 0.040$  Ma for the Cretaceous–Paleogene (K–Pg) and Danian–Selandian (D–S) boundaries respectively. Low sedimentation rates appear common in all records in the mid-Danian interval, including conspicuous condensed intervals in the oceanic records that in the past have hampered the proper identification of cycles. The comprehensive interbasinal approach applied here reveals pitfalls in time scale construction, filtering techniques in particular, and indicates that some caution and scrutiny has to be applied when building orbital chronologies. Finally, the Zumaia section, already hosting the Selandian Global Boundary Stratotype Section and Point (GSSP), could serve as the global Danian unit stratotype in the future.

© 2014 Elsevier B.V. All rights reserved.

## 1. Introduction

The use of cyclic sedimentary sequences originated from astronomical climate forcing has become a main tool for highly accurate age calibration and the construction of the modern Geological Time Scale (Gradstein et al., 2012). The record of the periodic variations of solar insolation changes provides a high-resolution built-in “metronome” that yields relative time scales and entails accu-

rate correlations. Astronomical tuning of these sequences to precise orbital solutions has led to unprecedented resolution in the geological record for the youngest part of the Cenozoic. In contrast, tuning the Early Paleogene has remained difficult despite new complete numerical solutions for the solar system (Varadi et al., 2003; Laskar et al., 2004), due to uncertainties and limitations inherent in the chaotic behaviour of the solar system and challenging radiometric age control (Laskar et al., 2011a, 2011b; Renne et al., 2013).

The first orbital tuning of the Danian interval based on a fully integrated astronomical solution was provided by Dinarès-Turell et al. (2003) (D03 from here on) studying the hemipelagic succession

\* Corresponding author. Tel.: +39 06 51860 387; fax: +39 06 51860 397.

E-mail address: jaume.dinare@ingv.it (J. Dinarès-Turell).

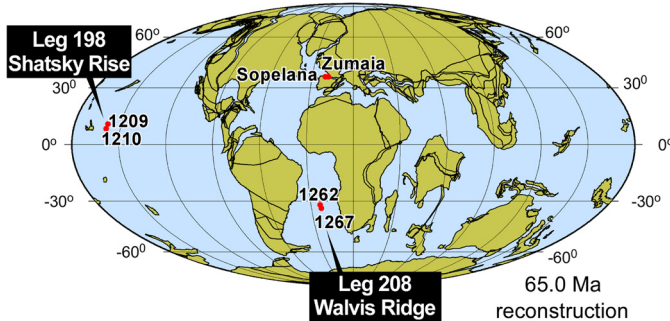


**Fig. 1.** Paleogeographic reconstruction for the early Paleocene (65 Ma) with location of marine ODP Sites and land-based sections used in this study.

at Zumaia (Fig. 1). Using the first full numerical astronomical solution Va03\_R7 (Varadi et al., 2003), the K-Pg boundary at Zumaia was tuned to an age of 65.83 Ma in D03. Subsequent integrated studies at Zumaia extended the orbital calibration to the entire Paleocene (Dinarès-Turell et al., 2007, 2010, 2012). The Paleocene tuning at Zumaia was revisited by Westerhold et al. (2008), Kuiper et al. (2008), and Hilgen et al. (2010) (W08, K08, and H10 respectively from here on) in light of a newly available solution (La2004; Laskar et al., 2004) and grounding the tuning on the stable ~405-kyr cycle. The favoured tuning option to La2004 in KU08 and H10 placed the K-Pg boundary at 65.95 Ma, which is basically the same age as in Dinarès-Turell et al. (2003) (the difference arising from the interpretation of an additional 100-kyr eccentricity cycle in the Zumaia record, see Fig. S1). This age was in accordance with the authors' new re-evaluation of the Fish Canyon sanidine (FCs) monitor standard, at 28.201 Ma. Subsequently, astronomical

tuning of ocean-drilling cores interpreting Pleistocene (Channell et al., 2010) and Paleocene to early Eocene records (Westerhold et al., 2012) resulted in different contentious estimates for the FCs standard. However, the key controversy for the Paleocene time scale stems from the number of ~405-kyr eccentricity cycles identified in the geological record along the Danian interval. Hilgen et al. (2010) contested the 24–405-kyr cycles for the entire duration of the Paleocene identified by Westerhold et al. (2008) in records from ODP Legs 198 (Shatsky Rise, North Pacific) and 208 (Walvis Ridge, South Atlantic) (Fig. 1), and proposed a total of 25 long eccentricity cycles instead. The additional cycle arises from a diverse interpretation of the involved deep-sea records in the Danian by H10 (Fig. 2). They further proposed a different correlation between the Atlantic Leg 208 and Pacific Leg 198 records of W08 that introduces considerable differences in age for a number of nannofossil bioevents (Fig. 2). Here, we reinvestigate the Danian orbital cycle stratigraphy at the land-based Zumaia section as well as the previously studied ODP Legs 198 and 208. We refine and reconcile the astronomical time scale for the lower Paleocene and present a robust correlation of bioevents and stable carbon isotope records between all investigated sites.

## 2. Material and methods

ODP Legs 198 (Shatsky Rise, NW Pacific Ocean) and 208 (Walvis Ridge, SE Atlantic Ocean) (Zachos et al., 2004; Bralower et al., 2006) (Fig. 1) provide the basis for an integrated stratigraphy and orbital tuning of the Cenozoic including the Paleocene (Westerhold et al., 2008). The basis for the Paleocene chronostratigraphy was mainly developed using non-destructive high resolution X-ray fluorescence (XRF) core scanner and core logging data from ODP Sites

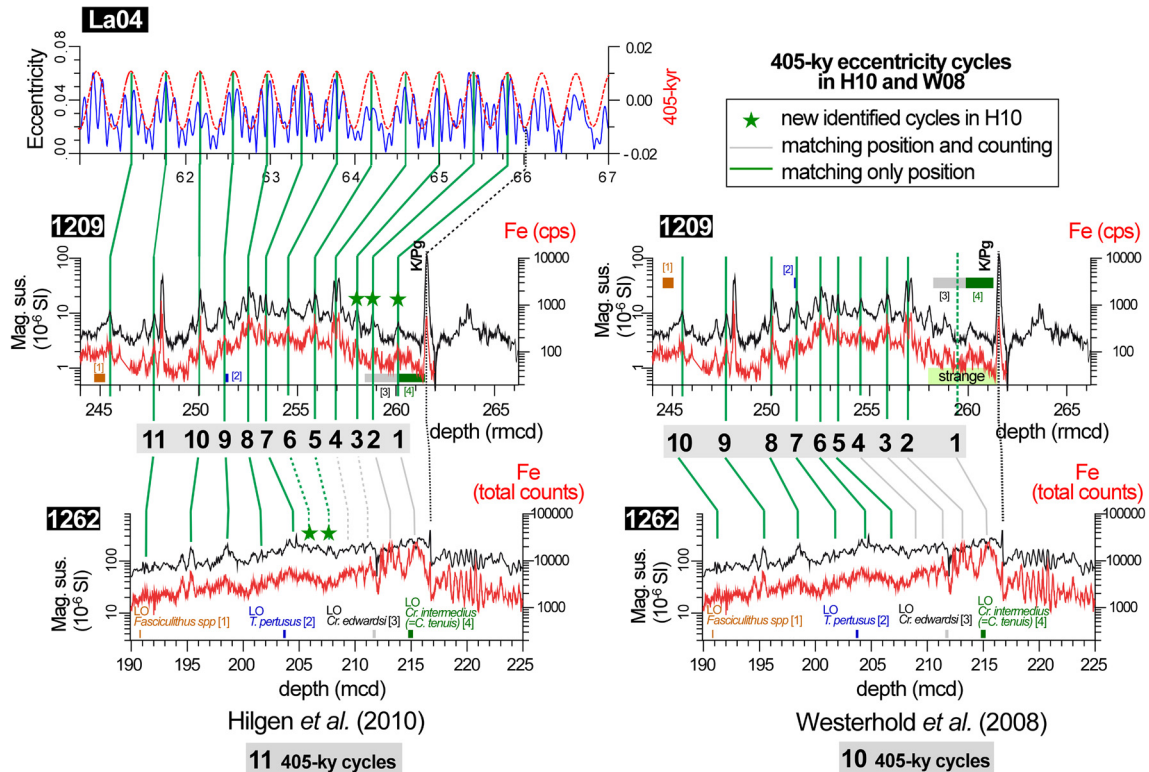


**Fig. 2.** Previous cyclostratigraphic interpretation and correlation of ~405-kyr cyclicity to magnetic susceptibility and Fe-counts in the lower Paleocene of ODP Leg 198 Site 1209 and ODP Leg 208 Site 1262. The tuning to eccentricity of the La04 (Laskar et al., 2004) as proposed in Hilgen et al. (2010) (H10) and the original correlation according to Westerhold et al. (2008) (W08) are shown. Note both the different number of identified ~405-kyr cycles and correspondence between the Atlantic and Pacific Sites. The small boxes above the depth axis of the records encompass the error bar of the given calcareous nannofossil biohorizon (data from Walvis Ridge sites as compiled/refined in Westerhold et al., 2008; Shatsky Rise sites are from Bralower et al., 2006): 1. LO *Fasciculithus* spp., 2. LO *T. pertusus*, 3. LO *C. edwardsii* (= *C. danicus* s.l.), 4. LO *Cr. intermedius* (= *C. tenuis* s.l.). The K/Pg boundary is indicated on the records and solid numbered lines mark the ~405-kyr cycles.

1209 through 1211 (Leg 198) and ODP Sites 1262, 1267 (Leg 208) (Westerhold et al., 2008). Here we define the iron (Fe) composite signal in a 2 cm resolution from Sites 1262 and 1209 as the representative master cores from the South Atlantic and North Pacific respectively. Magnetostratigraphy from Sites 1262 and 1267 was based upon shipboard paleomagnetic measurements conducted at 5 cm resolution augmented by discrete samples that were measured afterwards in the laboratory in order to refine the position of chron boundaries (Bowles, 2006; Westerhold et al., 2008). This has resulted in a highly reliable magnetostratigraphy usually resolved at <10 cm resolution for these two Atlantic Sites. Sites of Leg 198 in the Pacific lack a reliable magnetostratigraphy (Bralower et al., 2006) and, therefore, we have analysed 25 discrete samples from Site 1209 and 32 samples from Site 1210 in an attempt to define the magnetic polarity for the Danian interval. The benthic foraminiferal stable isotope record from Pacific ODP Site 1209 (Westerhold et al., 2011) and the bulk  $\delta^{13}\text{C}$  data from Walvis Ridge Site 1262 (Kroon et al., 2007) are used to guide the correlation of the records.

The Zumaia coastal-cliff section is a cyclic hemipelagic succession exposed along the Aitzgorri headland directly west of the town of Zumaia in the Basque Country, northern Spain. It represents a key section to define the late Cretaceous and Early Paleogene integrated chronostratigraphy (e.g., Dinarès-Turell et al., 2003) and includes the GSSPs (Global Stratotype Section and Points) of the Selandian and Thanetian Stages (Schmitz et al., 2011). In this study, bulk stable isotopes ( $\delta^{18}\text{O}$  and  $\delta^{13}\text{C}$ ) have been measured on 154 samples collected from the carbonate-rich layers of the basic precession couplets along the lower 35 m of the Danian strata from the Aitzgorri section. This new record is extended upwards by incorporating the data from the nearby Zumaia-Artadi section (Dinarès-Turell et al., 2012). In addition, the Danian part of the Sopelana section, about 60 km west from Zumaia (Fig. 3A), is studied for the first time in order to validate data available from Zumaia. A continuous 13-m long detailed log in Sopelana that encompasses Chron C28r (18 paleomagnetic samples) based on single bed and cycle identification allows unambiguous correlation to Zumaia and confirms previous results.

Paleomagnetic measurements have been gathered on a 2G Enterprises superconducting cryogenic magnetometer located in a shielded room at the Istituto Nazionale di Geofisica e Vulcanologia (INGV) in Rome (Italy). Discrete ODP samples were demagnetised stepwise by alternating fields (AF) up to 100 mT using coils installed in-line with the magnetometer. Samples from Sopelana were thermally demagnetised with a shielded Pyrox oven up to temperatures of 620 °C. Standard orthogonal demagnetisation diagrams and least-square fitting techniques were used to compute the magnetic components.

Composite core images for Sites 1209 and 1262 were assembled as an additional aid in correlation using an approach similar to Wilkens et al. (2009). For Site 1209 the digitised shipboard core images (Bralower et al., 2002) were used to construct a composite site image. For Site 1262 the line scan images taken on board with a GEOTEK MSCL XYZ track were assembled.

Stable isotope measurements on 155 freeze-dried powdered bulk sediment samples carefully selected from carbonate-rich limestones beds (not marly interbeds) at Zumaia from 0.96 to 35.19 m were performed on a Finnigan MAT 251 mass spectrometer equipped with an automated carbonate preparation line at the MARUM, University Bremen. The carbonate was reacted with orthophosphoric acid at 75 °C. Analytical precision based on replicate analyses of an in-house standard (Solnhofen Limestone) averages 0.05‰ (1 s) for  $\delta^{13}\text{C}$ . All data are reported against VPDB after calibration of the in-house standard with NBS-19. Bulk stable isotope data for Zumaia are reported in Table S1 and available at <http://doi.pangaea.de/10.1594/PANGAEA.835396>.

For time series analysis the software REDFIT version 3.8 has been employed (Schulz and Mudelsee, 2002). The software package by Torrence and Compo (1998) (<http://paos.colorado.edu/research/wavelets>) has been used for wavelet analysis. The continuous wavelet transform spectrum has been divided by its scales to account for a bias in the power spectrum (Liu et al., 2007).

### 3. Results

#### 3.1. Magnetostratigraphy

The Zumaia section encompassing the Danian interval (50 m of section above the K/Pg boundary) provides a good magnetostratigraphy integrated with calcareous plankton biostratigraphy (Dinarès-Turell et al., 2003). The position of the C27n/C26r reversal boundary was refined in Dinarès-Turell et al. (2010). Here we have studied a 13-m long Danian succession bounded by faults at Sopelana (Fig. 3) which can be correlated easily to the Zumaia section by using the clear pattern of lithological cycles (Fig. 3C and Fig. S2). Thermal demagnetisation of these samples (Fig. S3) identifies the characteristic primary remanence and allows the identification of C29n/C28r and C28r/C28n chron boundaries in agreement with the Zumaia data (Fig. 3C). Collectively, data indicate that C28r includes 12–13 precession cycles (note that polarity for precession cycle 48 could not be established, Fig. S2). The C29n/C28r reversal occurs just above the 100-kyr eccentricity minimum E11 while the C28r/C28n occurs close to the eccentricity maximum between E13 and E14 (Fig. 3D).

AF demagnetisation on discrete samples from Sites 1209–1210 produced demagnetisation diagrams with two magnetisation components (Fig. S4A). The first component is removed at fields below 20 mT while the characteristic component is defined in the range 20–100 mT. As those samples are geographically unoriented only the inclination value can be considered for magnetostratigraphic purposes. Unfortunately, when plotted on the depth scale no clear magnetostratigraphy emerges (Fig. S4B), and it must be concluded that the ChRM components in those samples must largely represent a remagnetisation.

#### 3.2. Cyclostratigraphic framework

Power spectra analysis (REDFIT) of the Fe-intensity reveals significant power at periods of about 1.2 m and 2.4 m for Sites 1209 and 1212 respectively (Fig. 4a). These periods mark the expression of the ~405-kyr cycle (E1) (Westerhold et al., 2008). Significant periods of 0.3–0.91 m and 0.7–0.9 m denote the expression of the short-eccentricity band (E2). These periods are consistent with the orbital frequencies (Fig. 4a) considering the diagnostic 1:4 ratio for short- and long-eccentricity.

Wavelet power spectra allow the visualisation of shifts of these spectral bands along depth that detect variations in sedimentation rates along the studied intervals of Sites 1209 and 1262 (Fig. 4b). In a distinct interval in the middle part at depths of about 250–255 rmcd for Site 1209 and 203–209 mcd for Site 1262 the spectral bands are less well defined as a result of lower sedimentation and/or condensation along these intervals. Interestingly, the weak spectral power at the corresponding precession band is barely significant on the global spectrum (Fig. 4a). In contrast, significant power at the precession band is obvious in the wavelet power spectrum at discrete intervals denoting higher amplitude of the precession cycles along those intervals as a result of the eccentricity modulation. These intervals of higher amplitude variations along the precession band correspond to the inferred ~405-kyr eccentricity maxima (Pc<sub>405.1</sub>–Pc<sub>405.11</sub>) the position of which is marked in Fig. 4b. The upper three eccentricity maxima appear well defined particularly for Site 1262. The other maxima

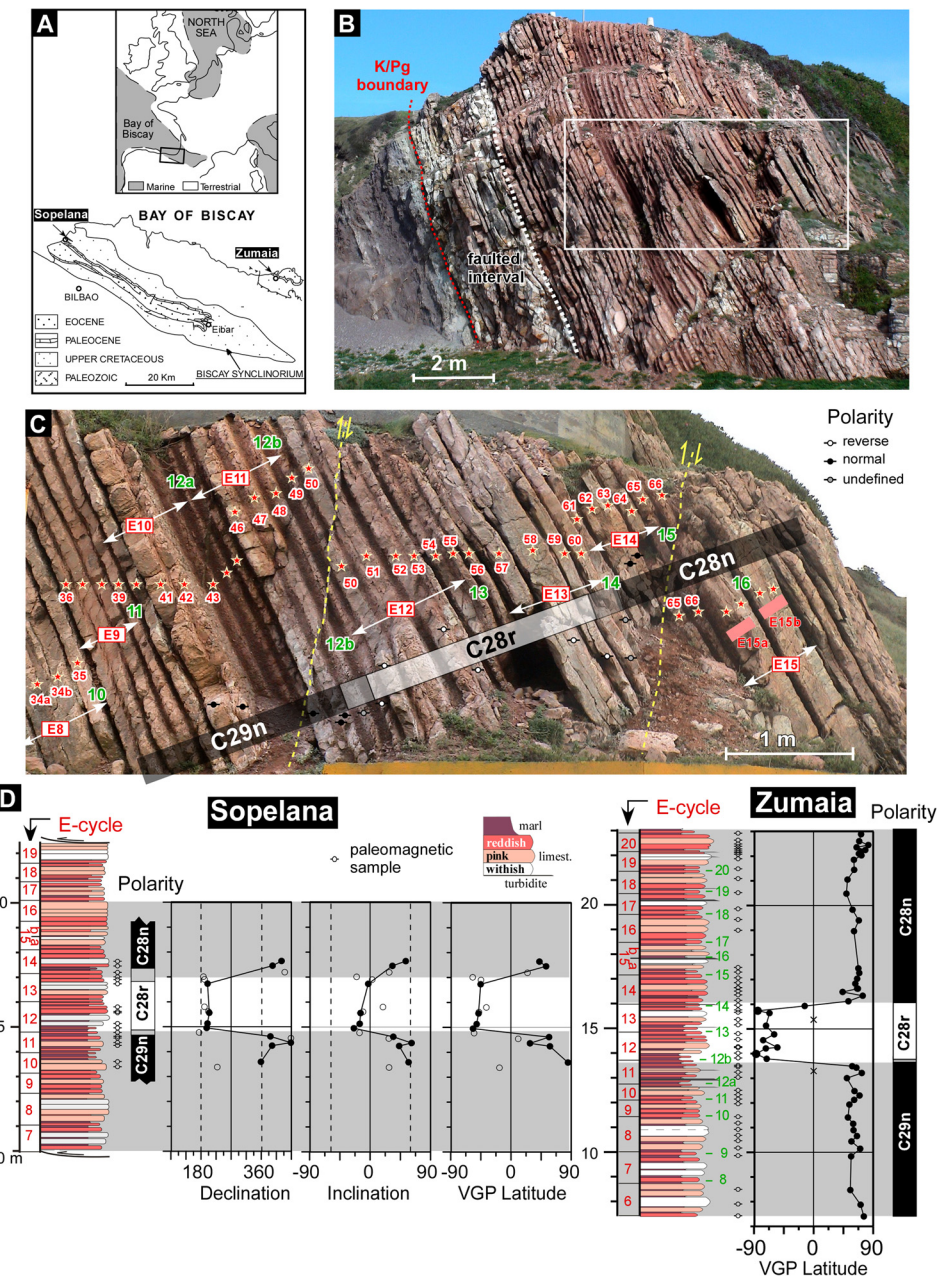


**Fig. 3.** Magnetostriatigraphy and cycle identification for the Sopelana section. A, location map; B, general field view of the analysed outcrop where the K/Pg boundary is outlined; C, detailed field view of the studied interval. Stars mark the carbonate-rich layer of the individual precession related couplets. These cycles and the 100-kyr eccentricity bundles (E-cycles) are labelled (red colour) following the nomenclature in Dinarès-Turell et al. (2003). The more marly intervals at the boundaries of the ~100-kyr E-cycles correspond to eccentricity maxima and the corresponding label (green colour) following the counting used by Westerhold et al. (2008) in the ODP records. Note the split eccentricity maxima 12a/12b and the E15a/E15b eccentricity minima as required by the synchronisation of the ODP records and Zumaia–Sopelana as proposed herein (see text for discussion); D, paleomagnetic results from Sopelana (this study) and comparison with results from Zumaia (Dinarès-Turell et al., 2003). (For interpretation of the references to colour in this figure legend, the reader is referred to the web version of this article.)

are less obvious, in particular in the central part of the records and in the lower part of Site 1209 as discussed below.

Because eccentricity modulates the precession signal's amplitude, the small-scale precession-related cycles are less well developed in the limestone beds of eccentricity-related cycles. This allows unambiguously inferring the phase relationship of the lithologic and astronomical cycles in a given succession. This criterion was employed on the Zumaia lithologic stacking pattern to infer that relatively marly rich intervals with well-developed small-scale precession-related couplets correspond to eccentricity maxima (Dinarès-Turell et al., 2003; Kuiper et al., 2008).

Here we present a new, improved correlation framework between the considered records resolved at the ~100-kyr eccentric-

ity cycle level which is coherent with the 405-kyr eccentricity cycles previously identified at Zumaia (Kuiper et al., 2008). We aim to obtain enhanced consistency among the records resulting in improved ages of the bio- and climatic events. We first carefully reassessed the cycle identification and correlation of the Zumaia and ODP Site 1262 records because both exhibit excellent magnetostriatigraphies for the studied Danian interval. These two records serve as master records. We aligned the magnetostriatigraphy and the cyclostratigraphies, defined visually, or by applying spectral analysis of published high-resolution X-ray fluorescence (XRF) core scanning and magnetic susceptibility records from the ODP site. The next step encompasses incorporating the other deep-sea record from the Pacific that lacks a reliable magnetostriatigraphy

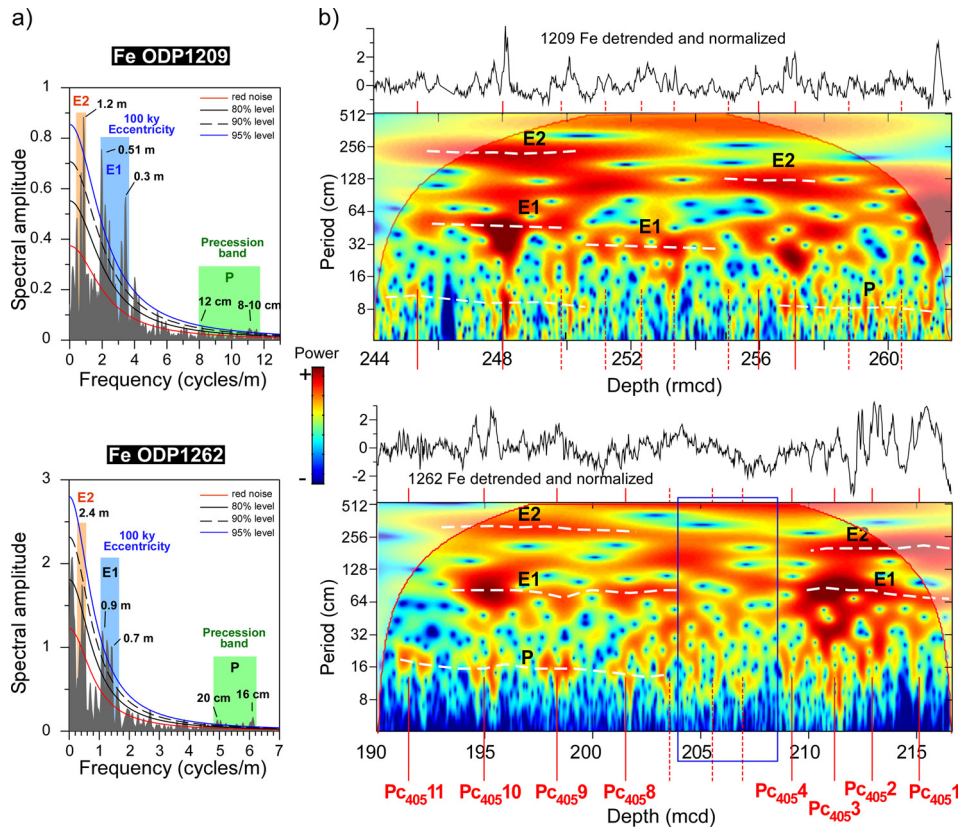


**Fig. 4.** Spectral analysis on the depth scale of the composite Fe intensity records for the early Paleocene intervals of ODP Sites 1209 (244–261.96 rmcd) and 1262 (190–216.59 mcd). A, spectra calculated with the REDFIT software on the respective log records. A linear trend was subtracted from 1262 data while data from 1209 was detrended by a sixth degree polynomial fit. Confidence levels based on a  $\chi^2$  distribution are calculated from the ARI-noise and from percentiles of the Monte Carlo ensemble. Three WOSA segments ( $N_{50} = 3$ ), 2000 Monte Carlo simulations ( $N_{sim} = 2000$ ) and a rectangular window ( $I_{win} = 0$ ) were applied. Relevant spectral peaks and associated eccentricity and precession bands are indicated; B, wavelet power spectrum using a Morlet wavelet. Shaded regions on either end indicate the cone of influence where edge effects become important. Dashed lines across the spectra mark the inferred ~405-kyr (E2), ~100-kyr cycle (E1) and ~21-kyr precession (P) cycles. The position of the PC<sub>405</sub>1 to PC<sub>405</sub>11 cycles is indicated. Dashed vertical lines on those cycles indicate their less obvious expression on the amplitude variations along the precession band.

raphy by focusing on the cyclic expression of the proxy records which is guided by core composite images (Fig. 5).

We maintained the ~100-kyr eccentricity minima and maxima numbering schemes of D03 and W08 respectively throughout the new correlation framework (Fig. 5). Whenever additional cycles were identified a subscript has been used. For instance, the excellent magnetostratigraphy for Site 1262 (Fig. 6A) made it possible to identify a previous unrecognised 100-kyr cycle at the base of Chron C28r between the previously identified eccentricity maxima 12 and 13 of W08 (Fig. 6B). The magnetostratigraphic data allows correlating the additional cycle to the Fe-intensity interval around 211 mcd resulting into that the original eccentricity maxima 12 defined cycle of W08 is split in two separate cycles (Fig. 6B).

The reasoning is as follows. At Zumaia–Sopelana the top of C28r (C28r/C28n reversal) occurs close to an eccentricity maxima situated between E13 and E14 eccentricity minima (Fig. 3) implying that this eccentricity maxima equals cycle 14 of W08 considering the magnetostratigraphy for Site 1262. Proceeding downward, at Zumaia–Sopelana, Chron C28r includes eccentricity bundle E12 with C29n/C29r located just above E11 with an uncertainty of one precession cycle (Figs. 3 and S1). At Site 1262, where precession cycles cannot be resolved, paleomagnetic data indicates that the low in Fe-intensity at 210.8 mcd is still characterised by reverse polarity, and therefore must correspond to the eccentricity minimum E12 (Fig. 6B). At the same time, the first Fe high with normal polarity at 211.4 mcd (cycle 12 of W08) should correspond to the eccentricity maxima below E11 at Zumaia, thus, requiring the interpretation of the additional eccentricity cycle at Site 1262

as outlined above. By doing this, both the cycle pattern and the magnetostratigraphy from the land based sections and Site 1262 is fully compatible for this interval. Note the conspicuous relatively marly character of the eccentricity maxima between E10 and E11 clearly visible at Sopelana (Fig. 3B, C), that matches the relative Fe-intensity high of cycle 12 of W08 at Site 1262 (Fig. 5).

The combined approach of considering paleomagnetic data, cyclic pattern and proxy records around C28n/C27r (Fig. 7) enables the identification of further previously unrecognised eccentricity cycles at the ODP Sites. The C28n/C27r reversal boundary is well defined just below the eccentricity maxima between E23 and E24 at Zumaia (Fig. 7A) and, hence, it can be correlated directly to eccentricity cycle 24 of W08 at Site 1262 (Fig. 7C). Nevertheless, in order to maintain the total number of 100-kyr eccentricity cycles within Chron C28n and conform to the ~405-kyr cycles pattern from Zumaia (Fig. 7A) (Kuiper et al., 2008), some revisions are required. At Site 1262, in the context of correlating this record to the land-based sections, we identify one previously unrecognised 100-kyr cycle in the upper part of C28n (original eccentricity maximum 22 from W08 is divided in two) (Fig. 7). Another cycle in the lower part of C27r is also split in two (cycle 25).

Additionally, the Zumaia section requires an extra 100-kyr cycle within C28n to maintain consistency with the number of short-eccentricity cycles at Site 1262 and the pattern of the ~405-kyr cycles which is not apparent at first glance. The necessity of this additional cycle at Zumaia agrees with the difference in tuning of the lower part of the section to one short-eccentricity cycle older by Kuiper et al. (2008) with respect D03 as imposed by

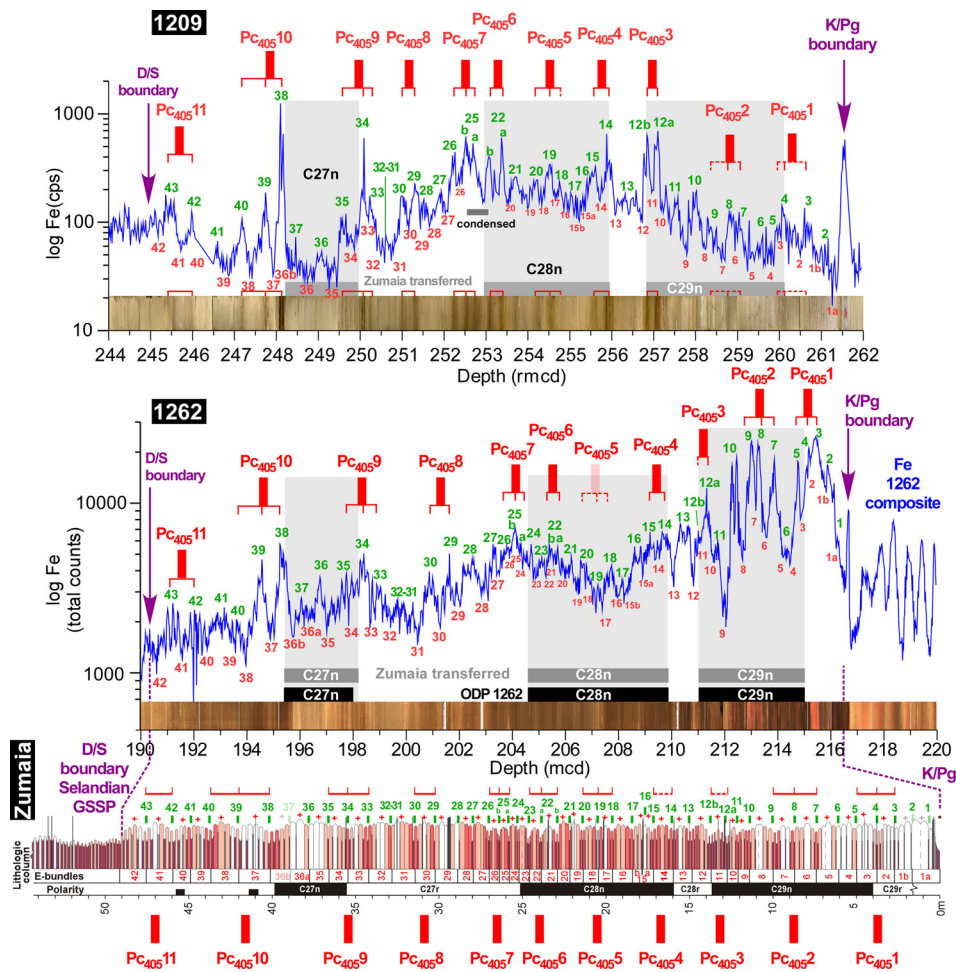


**Fig. 5.** Eccentricity correlation framework proposed in this study between the Zumaia succession and the ODP Sites 1209 (NE Pacific) and 1262 (SW Atlantic). The red numbers on the lows of the Fe curves on their respective depth scale for Sites 1209 and 1262 (top two panels) indicate the D03 correlated ~100-kyr eccentricity minima from Zumaia. The ~100-kyr original eccentricity maxima numbering from W08 (green numbers on the Fe curve highs) are maintained. Letter subscripts are added for newly identified cycles and are also plotted on the Zumaia lithologic log. Magnetostratigraphy from Site 1262 is fully compatible with that of Zumaia on this framework. Core composite images for both ODP Sites are included. Thick red bars including two or three well developed ~100-kyr eccentricity maxima (usually represented by dark intervals on the core images) correspond to ~405-kyr eccentricity maxima and are labelled PC<sub>405</sub>1 to PC<sub>405</sub>11 across the records (see text for discussion). (For interpretation of the references to colour in this figure legend, the reader is referred to the web version of this article.)

the match to the ~405-kyr eccentricity (Fig. S1). The extra cycle may be identified in bundle E15 of D03. Cycle E15 consists of two consecutive conspicuous carbonate-rich double couplets (Figs. 3 and S2). Prominent carbonate-rich couplets with relatively undeveloped marly interlayers are common on many eccentricity-minima related bundles. However, the stacking of two consecutive such packs of couplets as in E15 is unusual. We suggest that bundle E15 may actually be composed by two weakly developed ~100-kyr cycles and we have labelled them E15a and E15b accordingly (Figs. 3 and 5).

The correlation of the ~100-kyr cycles along PC<sub>405</sub>8 and above is straightforward (Fig. 5). A detailed discussion for this interval from mid C27r up to the Danian/Selandian boundary has been provided by Dinarès-Turell et al. (2010). It has been inferred that original eccentricity maxima 32 and 31 of W08 have to be merged in a single 100-kyr cycle (labelled 32–31 in Fig. 5). Moreover, bundle E36 from Zumaia should be divided in two weakly developed short-eccentricity cycles (E36a and E36b) attending the position of Chron C27n and cycle correlation to Site 1262 (Dinarès-Turell et al., 2010).

In summary, our new cyclostratigraphic framework includes three new 100-kyr eccentricity maxima cycles outlined in Site 1262 (arising from subdividing cycles 12, 22 and 25 from W08). All cycles have been recognised in Site 1209 with the exception of cycles

23–24 that conform a condensed interval. The identification/numbering of the eccentricity cycles in the lower 8 m of Site 1209 (cycles 1–22b) is substantially diverse from the interpretation in W08. At Zumaia, newly defined eccentricity minima cycles include the subdivision of original cycles E1, E15 and E36 from D03.

Taking the envisaged correlation framework outlined above (Fig. 5), the ODP records have been scaled to the Zumaia depth scale using ~100-kyr eccentricity maxima as tie points (Table S2). The scaled Fe-intensity,  $\delta^{13}\text{C}$  isotope records and composite core images for Sites 1209 and 1262 are plotted in Fig. 8 on the Zumaia lithological log and bulk isotope data for the section for comparison purposes (see also Fig. S5 for the isotope data plotted on the original depth scale for each record and also on a common age scale derived from the tuning to the La2011 orbital solution).

### 3.3. Bulk isotopes from Zumaia

The bulk stable carbon isotope data (Fig. S5A, Table S1) average  $1.77\text{\textperthousand}$  showing two shifts of  $0.3\text{--}0.4\text{\textperthousand}$  towards heavier values at 6 and 40 m. Pronounced variations with  $\sim 0.2\text{\textperthousand}$  amplitude related to the long (~405 kyr) eccentricity cycle can be observed in the data although the signal is not as clear as in the deep sea records. Bulk oxygen isotope values average  $-2.9\text{\textperthousand}$  revealing high amplitude variability of up to  $0.5\text{\textperthousand}$ . Because bulk oxygen values

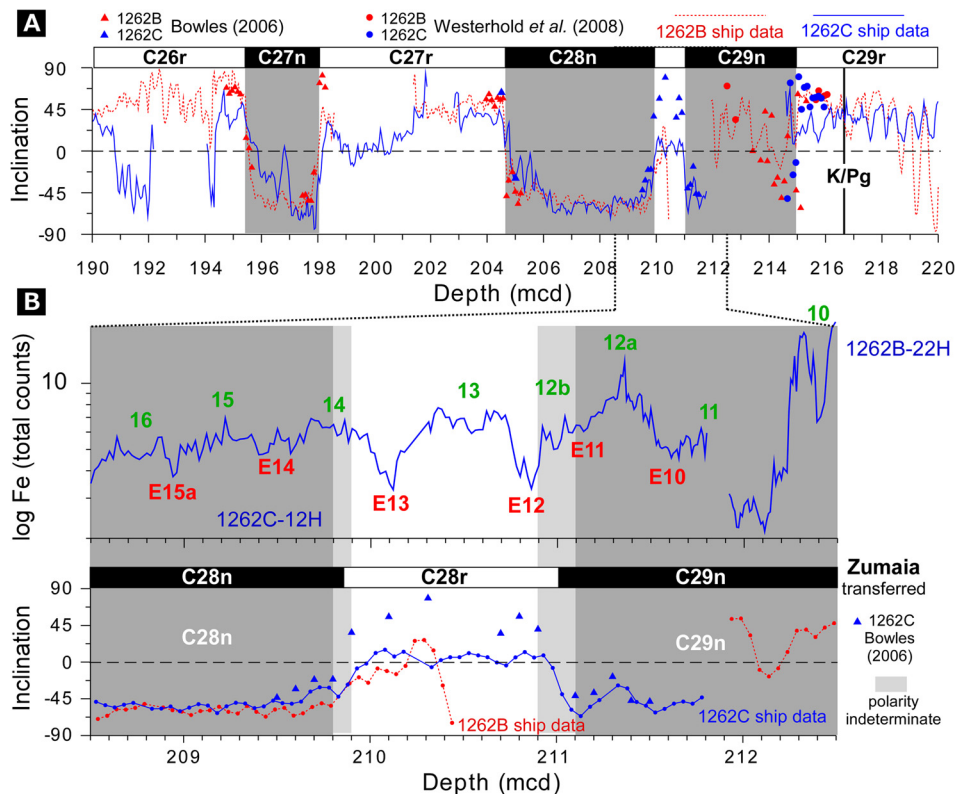


**Fig. 6.** Magnetostratigraphy for the 190–220 mcd interval for Site 1262 encompassing the Danian stage. A, shipboard pass-through inclination (demagnetised to 15 mT) for Hole 1262B (dashed) and 1262C (continuous) along with discrete sample inclination at 20 mT from Bowles (2006) (triangles) and Westerhold et al. (2008) (circles); B, enlargement for the interval that includes the C29n/C28r and C28r/C28n chron boundaries (208–213 mcd) plotted along the Fe XRF data and original eccentricity maxima of W08 for Site 1262 (green numbers on top). The eccentricity minima (E-cycles) (red labels) and magnetostratigraphy of D03 from Zumaia are correlated/transferred. (For interpretation of the references to colour in this figure legend, the reader is referred to the web version of this article.)

are very likely to be strongly altered by diagenesis we will not use it for correlation purposes.

#### 4. Discussion

##### 4.1. The Danian cyclostratigraphy and orbital tuning

A detailed lithological log using identification of single beds and 100-kyr eccentricity bundle cycles was produced for the Zumaia section in Dinarès-Turell et al. (2003) (D03). The carbonate-rich midpoint of those eccentricity-minima related bundles were numbered progressively from the K/Pg boundary upwards identifying a total of 42–100-kyr cycles in the interval (0–49 m) (Fig. S1). In a first attempt to tune the record, D03 correlated conspicuous carbonate-rich bundles E35–E36 to the node of low eccentricity amplitude driven by the ~2.4-My eccentricity modulation around 62 Ma in the Va\_R7 orbital solution. Then, D03 tuned all inferred eccentricity cycles in the record to successive minima in the solution. Kuiper et al. (2008) (K08) tuned the Zumaia record following a different approach. They visually analysed the expression of the ~405-kyr eccentricity cycles from the lithological log from D03 and in the field and attained almost an identical tuning compared to D03 (Fig. S1). Westerhold et al. (2008) (W08) reinterpreted the Zumaia stacking pattern to correlate to their inferred eccentricity cycles in the ODP records. Their approach for the identification of the eccentricity cycles in the ODP records largely relied on filtering the Fe-intensity record. They correlated the cyclicity of the 49 m Danian section at Zumaia to 46 eccentricity-maxima cycles above the K/Pg in their deep-sea records. Hilgen et al. (2010) (H10) noticed some discrepancies in the interpretation of W08 regarding the consistency in the number of ~100-kyr and ~405-kyr cycles. In particular, they noted that the minimum number of 112

precession-related cycles between the K/Pg boundary and the top of Chron C28n defined at Zumaia (D03) is not in accordance with the number of five ~405-kyr cycles inferred for the same interval of the Walvis Ridge sites. H10 further attempted to newly correlate the records of the Atlantic and Pacific ODP Sites. Their interpretation substantially diverges from that proposed by W08 (Fig. 2). However, this new interpretation results in poor correlation of several bioevents and climatic features (see discussion below).

The correlation framework outlined in Fig. 5 has focused on allowing the magnetostratigraphy and cyclic stacking pattern be compatible both at the long (~405-kyr) and short (~100-kyr) eccentricity cycles for these records. Previous correlation schemes largely relied on the extraction of the orbital cycles by spectral analysis and band-pass filtering (Westerhold et al., 2008; Hilgen et al., 2010). The applied filters had to account for inferred variations in sedimentation rates or cycle thickness along the records, thus, defining discrete intervals for the extraction. The Danian was separated in two intervals where different filters were used in W08 (176–204 mcd and 204–217 mcd for Site 1262; 236–250 rmcd and 250–261 rmcd for Site 1209). In fact, relying too heavily on the filters rather than the raw data may lead to incorrect or failed identification of cycles namely where minor variations in sedimentation rate or hiatuses/condensation occur. This seems sometimes unavoidable even when filters are carefully defined. W08 further encountered problems in the lower part of the Danian in Site 1209 where they defined a “strange interval” and assumed that one ~405 kyr was lacking expression (Fig. 2). This interval was reanalysed and challenged by H10 who identified three ~405-kyr cycles just above the K/Pg boundary in the interval 257–261 rmcd (Fig. 2). Although the spectral/filtering analysis of H10 of the lower Danian data from Site 1209 appears robust, it leads in the following to an incorrect correlation to the Site 1262 record. Their identification of

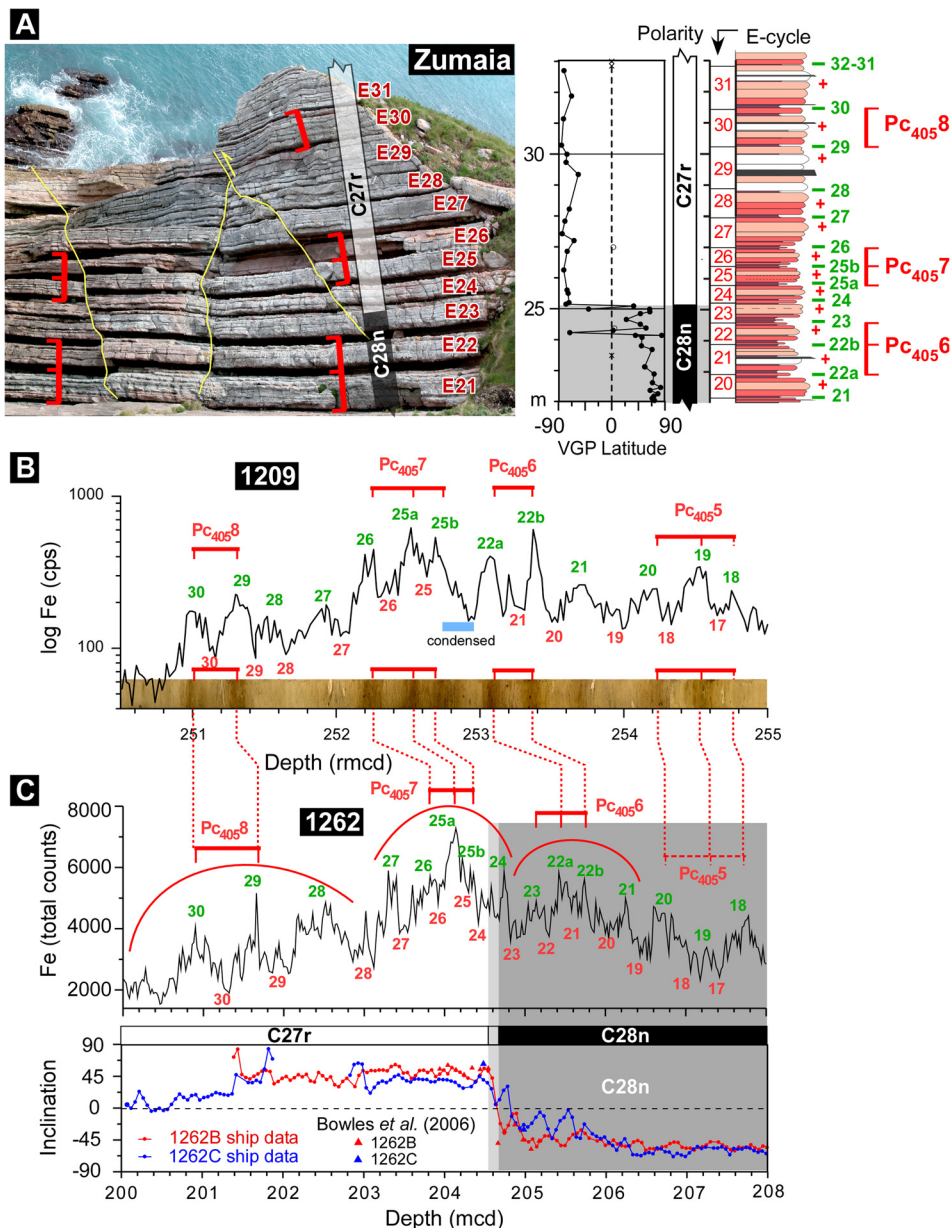


**Fig. 7.** Magnetostratigraphy and correlation around the C28n/C27r chron boundary. A, field view and magnetostratigraphic results from Zumaia (Dinarès-Turell et al., 2003); B, Fe-intensity record for the interval 250.5–255 rmcd from Site 1209 along the core image composite; C, Fe-intensity record and magnetostratigraphic results for the interval 200–208 mcd from Site 1262. The 100-kyr eccentricity minima or E-cycles from D03 (red numbers) and the reinterpreted eccentricity maxima from W08 (green numbers) are indicated across records. The 405-kyr eccentricity cycles Pctb4056,  $Pc_{405}6$  and  $Pc_{405}6$  as identified in this study are also shown. (For interpretation of the references to colour in this figure legend, the reader is referred to the web version of this article.)

three ~405-kyr cycles in the lower part resulted into a 405-kyr cycle mismatch between the Atlantic and Pacific Sites (see discussion below). Here, we challenge both W08 and H10 interpretations for this interval and propose two instead of three ~405-kyr cycles which aligns the cyclic pattern in Sites 1209 and 1262 below our  $Pc_{405}3$  cycle (Fig. 5). The conspicuous 2–3 dark layers having high Fe intensity values correspond with prominent short-eccentricity cycles (Fig. 5). Those high-amplitude cycles are indicative for the ~405-kyr eccentricity maxima and are used as guides to define cycles  $Pc_{405}3$ – $Pc_{405}11$  at Site 1209 (Fig. 5). These dark-layers appear rather blurred in the lower Danian, making our correlation along that interval less definite. However, cycle patterns of the Fe-intensity records from both sites correlate nicely. Relative high values for short-eccentricity maximum 10 in both records, interpreted close to a ~405-kyr minimum in our framework, lead in H10 to the addition of an ~405-kyr cycle (their number 3, Fig. 2).

Their filtering strategy even picks-up a further discrepant “extra” unnumbered cycle in Site 1210 along this interval. Recognised by them as unrealistic illustrates the shortcomings and difficulties of the filtering approach itself. Additionally, carbonate dissolution can produce high Fe peaks not necessarily driven by eccentricity cycles (the PETM is an extreme example). The lower Danian problematic part in Site 1209 is condensed in Site 1211 (Bralower et al., 2006). Henceforth, it remains a possibility that strong shoaling in Calcium Compensation Depth (CCD) contributes as driving mechanism to produce/enhance some of the Fe peaks in Site 1209. In this scenario, it is clear that extracting orbital cycles by spectral analysis/filtering alone would be hampered and misleading.

For tuning purposes one has to rely on the long-eccentricity cycle due to its stability far back in time (Varadi et al., 2003; Laskar et al., 2004). The short-eccentricity cycle is unreliable beyond 50 Ma in the most recent orbital solutions owing to the

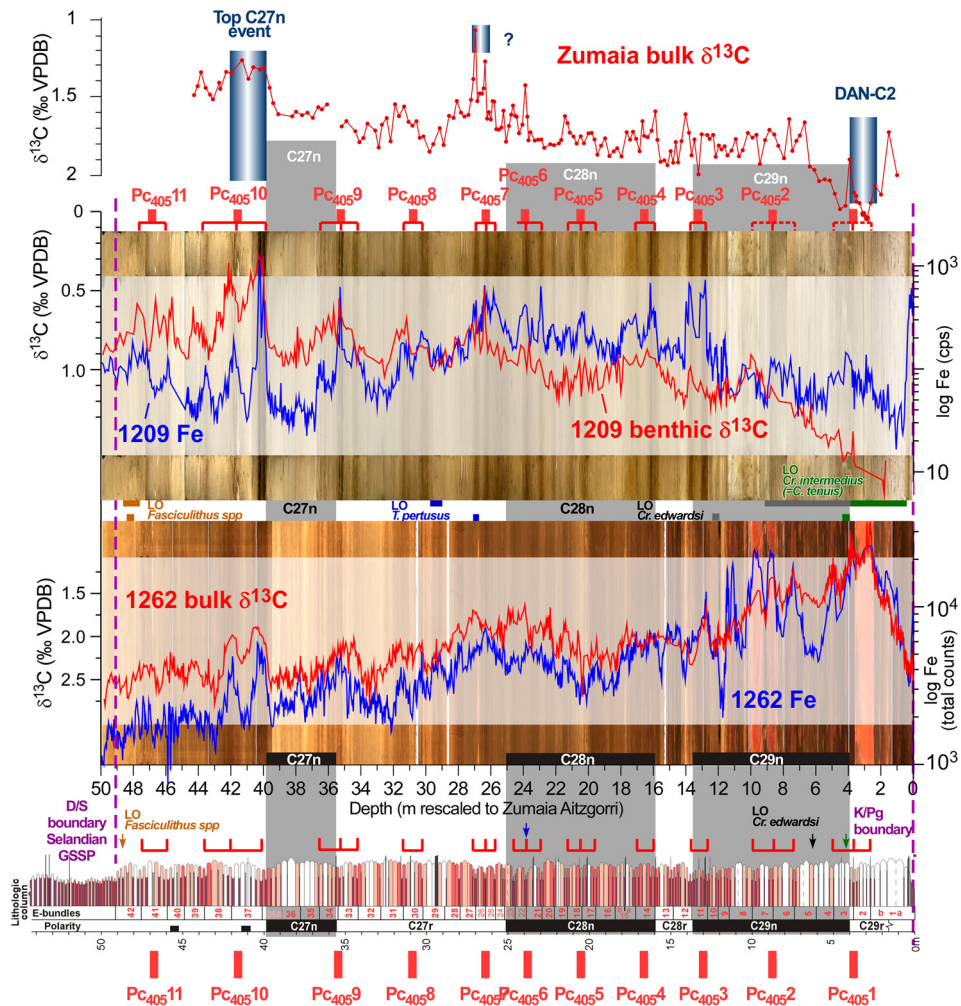


**Fig. 8.** Stable isotope data ( $\delta^{13}\text{C}$ ) and Fe intensity records for the early Paleocene intervals of ODP Sites 1209 (244–261.96 mcd) and 1262 (190–216.59 mcd) along the core image composite transferred to Zumaia depth using the age model presented herein. The aligned position of the PC<sub>405</sub>1 to PC<sub>405</sub>11 cycles, the K/Pg and D/S boundaries across the records is indicated. Calcareous nannofossil bioevents are also indicated. Top panel is the bulk  $\delta^{13}\text{C}$  data from Zumaia. Blue bars mark the Top Chron C27n (TC27n) and inferred DAN-C2 (Quillévéré et al., 2008) hyperthermal events. (For interpretation of the references to colour in this figure legend, the reader is referred to the web version of this article.)

chaotic behaviour of the inner Solar System (Laskar et al., 2011a). A stability test on the La2010 and La2011 set of orbital solutions carried out by Westerhold et al. (2012) suggests that only the La2010d and La2011 nominal solutions should be used beyond  $\sim 47$  Ma. Consequently, the  $\sim 405$ -kyr eccentricity beat is here used as a first order tuning for the Danian interval. Choosing the appropriate cycle in the astronomical solution is dictated by the numerical age of  $66.043 \pm 0.043$  Ma for the K/Pg boundary as established by  $^{40}\text{Ar}/^{39}\text{Ar}$  dating in the most recent study (Renne et al., 2013), and the fact that the boundary occurs close to a  $\sim 405$ -kyr eccentricity minima (e.g., Westerhold et al., 2008; Kuiper et al., 2008). The La2010d and nominal La2011 orbital solutions for the interval 59–69 Ma are plotted in Fig. 9 where the very long eccentricity cycle is marked by nodes of low amplitude in the solutions. The modulation of the 405 kyr component is caused by the  $g_4-g_3$  beat (related to the precession of the perihelion of the Earth and Mars), of period  $\sim 2.4$  My (Laskar et al., 2011a). Remarkably, these two solutions appear to be consistently sharing these low amplitude nodes back to a node at about 60 Ma where they start to diverge for about 8 My until a common node at about 68.1 Ma (Fig. 9). As indicated by Laskar et al. (2011a), it becomes clear that the long periodic terms related to  $g_4-g_3$  in the eccentricity are some key macroscopic features of the orbital solution that are imprinted in the geological record (Pälike et al. 2004;

Westerhold et al., 2012). Their precise recovery can, thus, provide some clues about the past chaotic diffusion of the orbital motion of the Earth and discriminate between alternative orbital solutions. It follows, that the Danian interval (roughly 66–62.5 Ma) together with the uppermost Maastrichtian is a suitable interval at least to test which astronomical solution best fits the geological data.

Considering the K/Pg boundary age constraints and the  $\sim 405$ -kyr cycle pattern we have tentatively tuned all the  $\sim 100$ -kyr maxima defined in the studied records to the La10d and La11 orbital solutions (Fig. 9 and Table S2). Spectral analysis of the tuned Fe-intensity data (Figs. S6, S7) produces significant peaks at the corresponding short and long-eccentricity periods which are maintained throughout the entire record (compare to Fig. 4). As we tuned to the short eccentricity, only amplitude variations along this band and power at the 405-yr period are significant. Focusing on the  $\sim 100$ -kyr eccentricity band on the wavelet spectra it can be noticed that there is an interval at about 64.1–64.3 Ma with depressed power indicating the presence of eccentricity cycles with relative lower amplitude (Figs. S6, S7). That interval comprises eccentricity maxima 14–21 (Fig. 9) showing a better fit with the La11 solution that contains a low-amplitude node in that age range. Weakly developed eccentricity cycles E15a–E15b and E36a–E36b at Zumaia correspond to particularly poor defined cycles in La11 that are linked to the 2.4 My very-long eccentricity minima (Fig. 9)

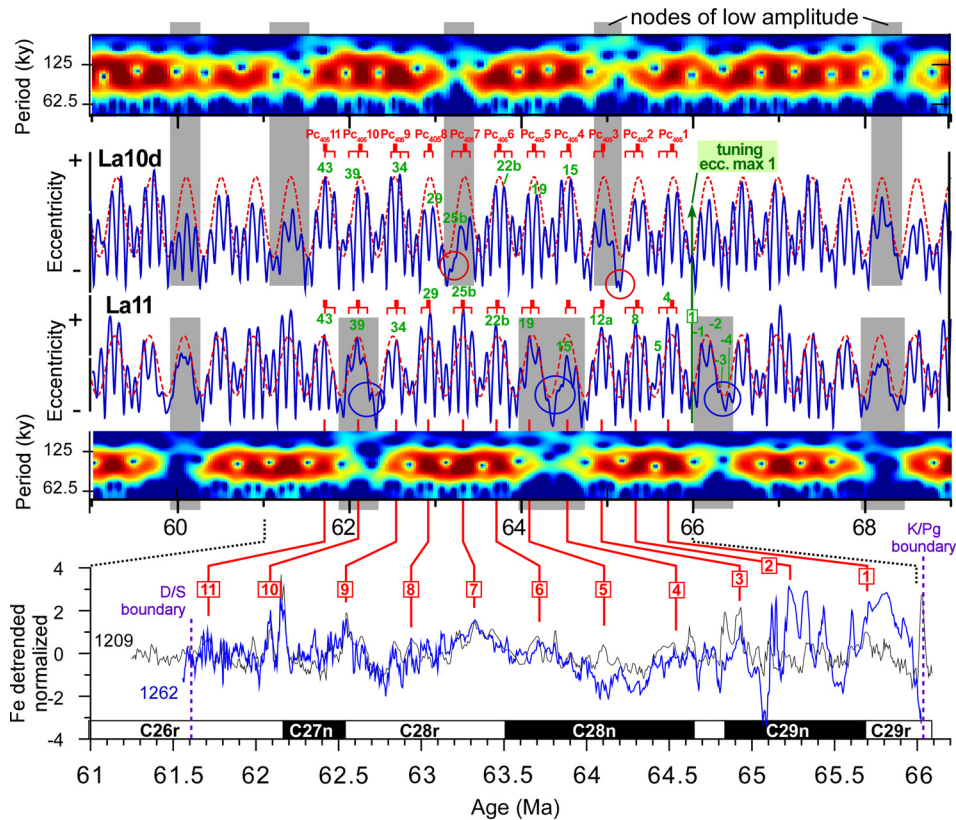


**Fig. 9.** The La10d (Laskar et al., 2011a) and La11 (Laskar et al., 2011b) eccentricity orbital solutions for the interval 59.5–68.5 Ma. Tuning of the eccentricity maxima as defined from the correlation of the Zumaia section and Site 1262 is shown on both solutions. The wavelet spectrum for a window of periods that visualise the ~100-kyr eccentricity amplitude variations is shown for each orbital solution. Nodes of relative low amplitude modulation in the eccentricity are marked by shaded bands. Circles on the solutions mark some intervals with weakly developed ~100-kyr cycles related to the long-term amplitude modulation. The bottom panel plots the detrended and normalised Fe records for Sites 1209 and 1262 as tuned to the La11 solution. The 11 Danian 405-kyr cycles and the corresponding magnetostratigraphy are indicated.

pointing to a remarkable consistency between geological data and the orbital solution. The low-amplitude node at about 62.1 Ma in La11 is also present in the Va03\_R7 orbital solution used in D03 to tune the conspicuous carbonate-rich eccentricity bundles E35–E36 from Zumaia. Moreover, the low-amplitude node at about 66.2 Ma just below the measured age for the K/Pg boundary matches relative low amplitude cycles for lithological Unit 12 just below the boundary at Zumaia (see Fig. 7 in Dinarès-Turell et al., 2013). In this uppermost Maastrichtian interval the faintly developed short-eccentricity maxima –3 and –4 from W08 (Fig. 4 in Westerhold et al., 2008) correspond to low-amplitude precession cycles that fit particularly weak eccentricity cycles in the La11 solution (Fig. 9). Collectively, all these evidences indicate that the La11 solution produces a better fit than the La10d solution on the studied records.

The new chronological framework, spanning a duration of about 4.5 Myr, allows assessing the role of orbital forcing on the paleoclimatic variability as registered by the relevant stable isotope records. These records (i.e. Sites 1262 and 1209) show dominance of the 100-kyr and 405-kyr eccentricity cycles (Figs. S6–S7) confirming that the carbon cycle and deep-sea temperature variations are dominated by orbital forcing as already inferred by Westerhold et al. (2011).

#### 4.2. The age of the K/Pg and D/S boundaries and the Danian time scale

The ages of 65.83 Ma (D03) and 65.94 Ma (K08/H10) were derived by tuning the oldest eccentricity minima in the Paleocene (E1 in D03) to the Va\_R7 orbital solution as explained above and adding ~2.5 precession cycles with average duration of ~21 kyr (Fig. S1). More recently, the same tuning approach has been used in Renne et al. (2013) who have considered the set of four solu-

tions (La10a–d and La11) from Laskar et al. (2011a, 2011b). These, yield astronomical ages for the K/Pg boundary ranging from 65.917 to 65.956 Ma. However, the lowermost Paleocene eccentricity bundle E1 from D03 was depicted dashed (Fig. A1 in Dinarès-Turell et al., 2003), denoting some uncertainty in its definition. In any case, a radiometric age close to 66 Ma for the K/Pg boundary has been confirmed by new high-precision  $^{40}\text{Ar}/^{39}\text{Ar}$  dating on tektites and bentonites associated with the boundary (Renne et al., 2013), while a three-way ( $^{40}\text{Ar}/^{39}\text{Ar}$ , U–Pb dating and astrochronology) intercalibration in the Cretaceous (Sageman et al., 2014) supports the astronomically calibrated age for the FCs standard value from K08 used to recalculate the radiometric age of the boundary.

The integrated correlation scheme presented herein suggests that the original eccentricity bundle E1 at Zumaia may actually represent two ~100-kyr cycles (E1a and E1b in Fig. 5), which was already inferred by W08. However, the detailed arrangement of the precession-related couplets within that interval is ambiguous. Consequently, the accuracy of any astronomical calibration of the K/Pg boundary based on the lowermost Paleocene strata remains somewhat tentative. In fact, it may be better at this moment to infer the astronomical age of the K/Pg boundary on the cyclic patterns from the uppermost Maastrichtian instead. The carbonate record from the uppermost 65-m Maastrichtian strata at Zumaia (ten Kate and Sprenger, 1993) was reanalysed by Dinarès-Turell et al. (2013) that clearly extracted both the short and long-eccentricity cycles much in accordance with cyclostratigraphic analysis based on magnetic susceptibility and colour reflectance by Batenburg et al. (2012) along that interval. The youngest Maastrichtian ~405-kyr eccentricity minima occurs at about 14 m below the K/Pg boundary, interval that includes about four ~100-kyr cycles, confirming the notion that the K/Pg boundary is located close to a 405-kyr min-

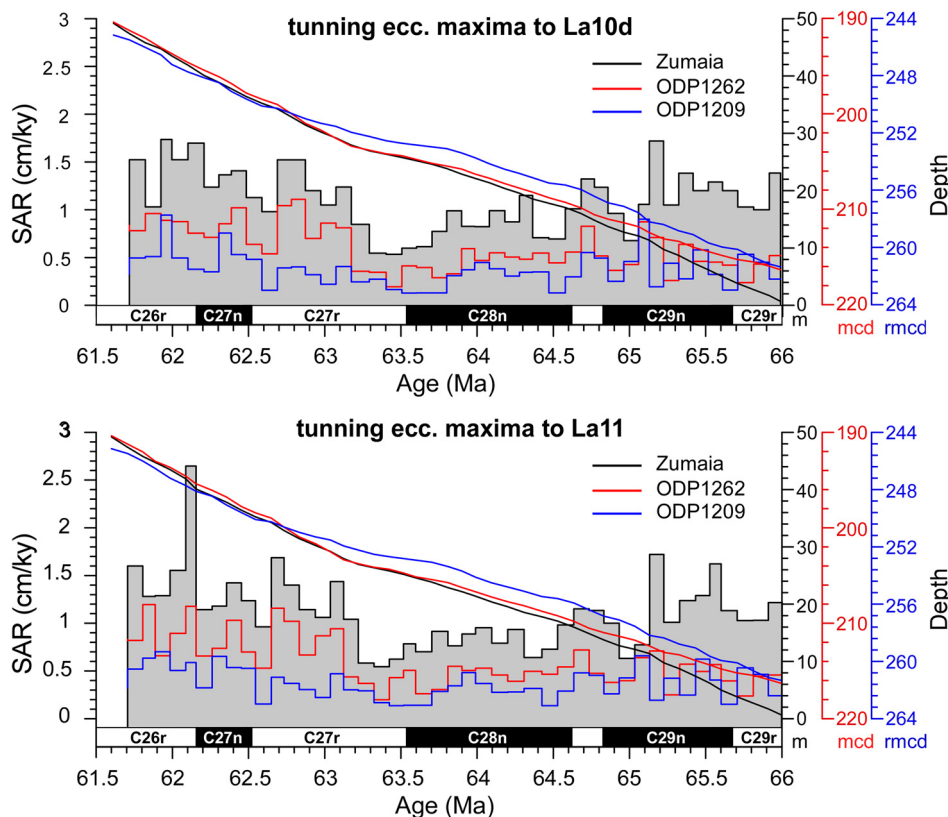


**Fig. 10.** Sediment rates (SARs) derived for the short-eccentricity maxima calibrated records from Walvis Ridge (1262, red), Shatsky Rise (1209, blue) and Zumaia (black) plotted along the age axis and calibrated magnetostratigraphy of this study. Tuning options to the La10d (top) and La11 (bottom) orbital solutions are shown. (For interpretation of the references to colour in this figure legend, the reader is referred to the web version of this article.)

imum. The first eccentricity maxima below the K/Pg occurs 3–4 precession cycles below the boundary at Zumaia (Dinarès-Turell et al., 2013) and by tuning to the corresponding maxima in the La11 solution (66.096 Ma) and subtracting ~3.5 precession cycles, an age of  $66.0225 \pm 0.0040$  Ma can be derived for the K/Pg. This age is in agreement with the astronomical age of  $66 \pm 0.07$  Ma of Husson et al. (2011) (option 2) derived from Maastrichtian sediments from deep-sea cores and the preferred absolute age of  $66.043 \pm 0.043$  Ma from Renne et al. (2013).

The astronomical age for the D/S boundary ( $61.6075$  Ma  $\pm 40$  kyr) is established by tuning the youngest eccentricity maxima (E42) to the corresponding maxima in the La11 orbital solution, which is our preferred solution, and subtracting ~2.5 precession cycles. Consequently, the duration of the Danian stage can be estimated at  $4.415$  My  $\pm 80$  kyr.

Likewise, accurate astronomical tuned ages can be derived for the intervening Danian magnetic reversals and biostratigraphic events from each record using the corresponding age of the nearest short- or long-eccentricity maxima and minima as inferred in our framework (Tables S1–S2) and then using extrapolation or the counting of precession cycles when present. The position of the calcareous plankton events from Zumaia were listed in Dinarès-Turell et al. (2003) while the position of nannofossil events for Sites 1262 and 1209 were given in Westerhold et al. (2008). Table S4 gives our revised tuned ages for all these events along the W08 and H10 ages for comparison. To infer cross-site discrepancies we plot the main bioevents for each record along a common depth-scale (Fig. 8). It is beyond the scope of this study to discuss uncertainties in the lowermost Danian biostratigraphy that probably arise by a multiple factors including poor preservation/dissolution and differential sampling resolution. However, the strong diachroneity of successive nannofossil events from 61 and 63 Ma

as in the H10 age model is resolved based on our different identification and correlation of the ~405-kyr cycles. In our framework the age of the lowest occurrence (LO) of *Fasciculithus* spp. that approximates the D/S boundary (see discussions in Dinarès-Turell et al., 2010 and Monechi et al., 2013) is similar among the analysed records.

Astronomical tuned ages for the intervening Danian magnetic reversals and magnetochron durations are given in Table S5 and Table S6 respectively. We provide both a 405-kyr and a 100-kyr eccentricity based tuned scales. The long-eccentricity tuning should theoretically be more correct than the short-eccentricity tuning given the inaccuracy (due to chaotic behaviour of the Solar System) in the current 100-kyr astronomical solution. Nevertheless, determining the exact position of the 405-kyr cycles in the lithologic record is prone to some error and this would likely counterbalance the precision and stability of this periodicity in the astronomical solution. Our new age estimates produce values that are close to those from the GTS12 that are based in the 405-kyr tuning estimate of H10 from Site 1262 and usually within less than 50 kyr.

#### 4.3. Sedimentation rates and South Atlantic spreading rates

The variation of sedimentation rates for the studied records is derived from our tuning the short-eccentricity maxima to the La10d and La11 orbital solutions (Fig. 10). The Zumaia and the South Atlantic Site 1262 records reveal a consistent and thus global increase in sedimentation rates in the upper Danian at about 63.2 Ma. The lowest sedimentation rates appear to straddle the C28n/C27r reversal interval and lower Chron C27r where some condensation has been inferred for Site 1209. In the sequence stratigraphy scenario for the Basque Basin put forward by Pujalte et al. (1998) the lower parts of the 3rd-order depositional sequences display comparatively high-sedimentation rates

that are followed by condensed intervals. These condensed intervals were interpreted as the basinal expression of the transgressive systems tracts (TST) and separate, therefore, the lowstand (LS) (below) and highstand (HST) deposits. For the Danian interval under consideration, one such condensed interval is visualised by the relatively packed bundles (or “crowded” bundles of Pujalte et al., 1998) E21–E26 (Fig. 5). These are linked to their DS-P1 depositional sequence and correspond to the low sedimentation interval inferred from our tuned model along the 63.6–63.2 Ma interval (Fig. 10). The relative high sedimentation rates inferred for the upper Danian (63.2–61.5 Ma) (Fig. 10) thus correspond to the HST of the same depositional sequence. The similarity of the sedimentation rate patterns among the studied records from different basins would argue in favour of the global character of the involved depositional sequences thus suggesting a eustatic signature. The validity of this model and the ultimate driving mechanism deserves further insight and a broader time frame analysis.

Our estimates for the duration of Danian chrons (Table S6) based on tuning eccentricity do not differ substantially from the GTS12 derived estimates, particularly the 405-kyr cycle based option. For Chron C28r, the duration estimate of 177–187 kyr of W08 based on the short eccentricity that produced anomalously high spreading rates for the South Atlantic seafloor is here ameliorated (224 kyr) (Table S6) due to the identification of the additional short-eccentricity maxima 12b within C28r in the oceanic records as discussed above. However, in agreement with H10, we consider that for this short chron the best estimate is most likely the one based on counting the precession cycles from Zumaia (252–273 ky, Table S5).

## 5. Conclusions

We have revised the correlation between the land-based Zumaia section and deep-sea records from ODP Legs 198 (Shatsky Rise, North Pacific) and 208 (Walvis Ridge, South Atlantic) for the Danian interval. The new integrated framework, resolved at 100-kyr short-eccentricity resolution, shows a compatible magnetostratigraphy between Zumaia (here confirmed by new data from the Sopelana section) and the Leg 208 sites while maintaining consistent astronomically cycle stacking patterns of the short- and 405-kyr long-eccentricity cycles across records. Correlation to the Pacific Sites 1209–1210 is achieved by mostly visual inspection of the Fe-intensity records supported by core images composites that portray conspicuous clusters of dark layers related to the ~405-kyr eccentricity cycle maxima. The revised cyclostratigraphy allows the identification of three additional short-eccentricity cycles in the ODP records and it also helps to refine the interpretation of the Zumaia section. Our new data and integrated data approach now challenge the interpretation of Hilgen et al. (2010) for the Pacific Sites 1209–1210 for the lower Danian by a 405-kyr cycle. The results further reconcile biostratigraphic evidences for the Danian/Selandian boundary and stable isotope data track the top Chron C27n hyperthermal event across the oceans. The revised framework recognises 11 (and not 10 as in Westerhold et al., 2008) ~405-kyr cycles along the Danian Stage. The astronomically tuned ages of the K/Pg and the D/S boundaries are  $66.022 \pm 0.040$  Ma and  $61.607 \pm 0.040$  Ma respectively as derived from our preferred tuning to the La11 orbital solution. Alternative options to shift to either younger or older 405-kyr eccentricity cycles can be disregarded in the context of recent high resolution  $^{40}\text{Ar}/^{39}\text{Ar}$  and integrated U/Pb absolute dating studies (Renne et al., 2013; Sageman et al., 2014). The analysis of the modulation of the amplitude of the 405 kyr eccentricity term which translates in low-amplitude less-well defined short-eccentricity cycles allows discriminating between the La10d and La11 orbital solutions along the Danian with the latter resulting into a better fit with the

geologic data. Moreover, the new bulk-rock  $\delta^{13}\text{C}$  isotope record obtained at Zumaia at almost precession-cycle resolution for most of the Danian from the K/Pg boundary up to including Chron C27n is correlated to the equivalent record from Site 1262 (Kroon et al., 2007). The benthic record from Site 1209 (Westerhold et al., 2011) confirms that the carbon cycle and deep-sea temperature are dominated by orbital forcing mostly at the 405-kyr frequency. Finally, we propose a Danian global unit stratotype (in the sense of Hilgen et al., 2006) at Zumaia, where the Selandian GSSP is already defined.

Our high-resolution interbasinal integrated approach that combines proxy data from deep-sea records and examines the lithostratigraphy and associated magnetic-geochemical-biostratigraphic record of coeval marine sections in outcrops, has enabled to settle a long-standing conundrum in the astronomical calibration of the Early Paleogene. We have ascertained some drawbacks inherent to the application of common practices in cyclostratigraphy, such band-pass filtering, on some sedimentary successions than can lead to misleading results. We believe our contribution sets an example for future time scales development and extension of the orbital chronologies into the Cretaceous and should enlighten cyclostratigraphers and chronostratigraphers akin.

## Acknowledgements

The research was funded by project CGL2011-23770 of the Spanish Min. de Economía y Competitividad. JDT acknowledges a sabbatical grant (SAB2011-0045) from the Spanish Min. de Educación. The study used samples and data provided by the Integrated Ocean Drilling Program (IODP). The Deutsche Forschungsgemeinschaft (DFG) (grant RO 1113/5) and the MARUM – Center for Marine Env. Sci., Univ. of Bremen, are acknowledged for providing fiscal support. Julie Bowles is warmly thanked for sharing paleomagnetic data and insights from Leg 208. Positive and insightful reviews by Jim Ogg and two anonymous reviewers helped to sharpen the paper.

## Appendix A. Supplementary material

Supplementary material related to this article can be found online at <http://dx.doi.org/10.1016/j.epsl.2014.08.027>.

## References

- Batenburg, S.J., Sprovieri, M., Gale, A.S., Hilgen, F.J., Husing, S., Laskar, J., Liebrand, D., Lirer, F., Orue-Etxebarria, X., Pelosi, N., Smit, J., 2012. Cyclostratigraphy and astronomical tuning of the Late Maastrichtian at Zumaia (Basque country, Northern Spain). *Earth Planet. Sci. Lett.* 359, 264–278. <http://dx.doi.org/10.1016/j.epsl.2012.09.054>.
- Bernaola, G., Martín-Rubio, M., Baceta, J.I., 2009. New high resolution calcareous nannofossil analysis across the Danian/Selandian transition at the Zumaia section: comparison with South Tethys and Danish sections. *Geol. Acta* 7, 79–92.
- Bowles, J., 2006. Data report: revised magnetostratigraphy and magnetic mineralogy of sediments from Walvis Ridge, Leg 208. In: Kroon, D., Zachos, J.C., Richter, C. (Eds.), Proc. ODP, Sci. Results, vol. 208. Ocean Drilling Program, College Station, TX, pp. 1–24.
- Bralower, T.J., Premoli Silva, I., Malone, M.J., et al., 2002. In: Proc. ODP, Init. Repts., vol. 198. Ocean Drilling Program, College Station, TX.
- Bralower, T.J., Premoli Silva, I., Malone, M.J., 2006. Leg 198 synthesis: a remarkable 120-m.y. record of climate and oceanography from Shatsky Rise, northwest Pacific Ocean. In: Bralower, T.J., Premoli Silva, I., Malone, M.J. (Eds.), Proc. ODP, Sci. Results, vol. 198.
- Channell, J.E.T., Hodell, D.A., Singer, B.S., Xuan, C., 2010. Reconciling astrochronological and  $^{40}\text{Ar}/^{39}\text{Ar}$  ages for the Matuyama–Brunhes boundary and late Matuyama Chron. *Geochem. Geophys. Geosyst.* 11, Q0AA12. <http://dx.doi.org/10.1029/2010GC003203>.
- Dinarès-Turell, J., Baceta, J.I., Pujalte, V., Orue-Etxebarria, X., Bernaola, G., Lorito, S., 2003. Untangling the Palaeocene climatic rhythm: an astronomically calibrated Early Palaeocene magnetostratigraphy and biostratigraphy at Zumaia (Basque basin, northern Spain). *Earth Planet. Sci. Lett.* 216, 483–500. [http://dx.doi.org/10.1016/S0012-821X\(03\)00557-0](http://dx.doi.org/10.1016/S0012-821X(03)00557-0).

- Dinarès-Turell, J., Baceta, J.I., Bernaola, G., Orue-Etxebarria, X., Pujalte, V., 2007. Closing the Mid-Palaeocene gap: toward a complete astronomically tuned Palaeocene Epoch and Selandian and Thanetian GSSPs at Zumaia (Basque Basin, W Pyrenees). *Earth Planet. Sci. Lett.* 262, 450–467. <http://dx.doi.org/10.1016/j.epsl.2007.08.008>.
- Dinarès-Turell, J., Stoykova, K., Baceta, J.I., Ivanov, M., Pujalte, V., 2010. High-resolution intra- and interbasinal correlation of the Danian–Selandian transition (Early Paleocene): the Bjala section (Bulgaria) and the Selandian GSSP at Zumaia (Spain). *Palaeogeogr. Palaeoclimatol. Palaeoecol.* 297, 511–533. <http://dx.doi.org/10.1016/j.palaeo.2010.09.004>.
- Dinarès-Turell, J., Pujalte, V., Stoykova, K., Baceta, J.I., Ivanov, M., 2012. The Palaeocene “top chron C27n” transient greenhouse episode: evidence from marine pelagic Atlantic and peri-Tethyan sections. *Terra Nova* 24, 477–486. <http://dx.doi.org/10.1111/j.1365-3121.2012.01086.x>.
- Dinarès-Turell, J., Pujalte, V., Stoykova, K., Elorza, J., 2013. Detailed correlation and astronomical forcing across the Upper Maastrichtian succession from the Basque Basin. *Bol. Geol. Min.* 124, 253–282.
- Gradstein, F.M., Ogg, J.G., Schmitz, M.D., Ogg, G.M., 2012. *The Geological Time Scale 2012*. Elsevier. 1176 pp.
- Hilgen, F., Brinkhuis, H., Zachariasse, W.-J., 2006. Unit stratotypes for global stages: the Neogene perspective. *Earth-Sci. Rev.* 74, 113–125. <http://dx.doi.org/10.1016/j.earscirev.2005.09.003>.
- Hilgen, F.J., Kuiper, K.F., Lourens, L.J., 2010. Evaluation of the astronomical time scale for the Paleocene and earliest Eocene. *Earth Planet. Sci. Lett.* 300, 139–151. <http://dx.doi.org/10.1016/j.epsl.2010.09.044>.
- Husson, D., Galbrun, B., Laskar, J., Hinnov, L.A., Thibault, N., Gardin, S., Locklair, R.E., 2011. Astronomical calibration of the Maastrichtian (Late Cretaceous). *Earth Planet. Sci. Lett.* 305, 328–340. <http://dx.doi.org/10.1016/j.epsl.2011.03.008>.
- Kroon, D., Zachos, J.C., 2007. Leg 208 Scientific Party, 2007. Leg 208 synthesis: Cenozoic climate cycles and excursions. In: Kroon, D., Zachos, J.C., Richter, C. (Eds.), *Proc. ODP, Sci. Results, vol. 208. Ocean Drilling Program, College Station, TX, pp. 1–55*.
- Kuiper, K.F., Deino, A., Hilgen, F.J., Krijgsman, W., Renne, P.R., Wijbrans, J.R., 2008. Synchronizing rock clocks of Earth history. *Science* 320, 500–504. <http://dx.doi.org/10.1126/science.1154339>.
- Laskar, J., Robutel, P., Joutel, F., Gastineau, M., Correia, A.C.M., Levrard, B., 2004. A long-term numerical solution for the insolation quantities of the Earth. *Astron. Astrophys.* 428, 261–285. <http://dx.doi.org/10.1051/0004-6361:20041335>.
- Laskar, J., Fienga, A., Gastineau, M., Manche, H., 2011a. La2010: a new orbital solution for the long-term motion of the Earth. *Astron. Astrophys.* 532, A89. <http://dx.doi.org/10.1051/0004-6361/201116836>.
- Laskar, J., Gastineau, M., Delisle, J.-B., Farres, A., Fienga, A., 2011b. Strong chaos induced by close encounters with Ceres and Vesta. *Astron. Astrophys.* 532, L4. <http://dx.doi.org/10.1051/0004-6361/201117504>.
- Liu, Y., San Liang, X., Weisberg, R.H., 2007. Rectification of the bias in the wavelet power spectrum. *J. Atmos. Ocean. Technol.* 24, 2093–2102. <http://dx.doi.org/10.1175/2007JTECHO511.1>.
- Monechi, S., Reale, V., Bernaola, G., Balestra, B., 2013. The Danian/Selandian boundary at Site 1262 (South Atlantic) and in the Tethyan region: biomagnetostratigraphy, evolutionary trends in fasciculoliths and environmental effects of the Latest Danian Event. *Mar. Micropaleontol.* 98, 28–40. <http://dx.doi.org/10.1016/j.marmicro.2012.11.002>.
- Pálike, H., Laskar, J., Shackleton, N.J., 2004. Geologic constraints on the chaotic diffusion of the solar system. *Geology* 32, 929–932. <http://dx.doi.org/10.1130/G20750.1>.
- Pujalte, V., Baceta, J.I., Orue-Etxebarria, X., Payros, A., 1998. Paleocene strata of the Basque Country, western Pyrenees, northern Spain: facies and sequence development in a deep-water starved basin. In: de Graciansky, P.-Ch., Hardenbol, J., Jacquin, T., Vail, P. (Eds.), *Mesozoic and Cenozoic Sequence Stratigraphy of European Basins*. In: SEPM Spec. Publ., vol. 60, pp. 311–325.
- Quillévéré, F., Norris, R.D., Kroon, D., Wilson, P.A., 2008. Transient ocean warming and shifts in carbon reservoirs during the early Danian. *Earth Planet. Sci. Lett.* 265, 600–615. <http://dx.doi.org/10.1016/j.epsl.2007.10.040>.
- Renne, P.R., Deino, A.L., Hilgen, F.J., Kuiper, K.F., Mark, D.F., Mitchell III, W.S., Morgan, L.E., Mundil, R., Smit, J., 2013. Time scales of critical events around the Cretaceous–Paleogene boundary. *Science* 339, 684–687. <http://dx.doi.org/10.1126/science.1230492>.
- Sageman, B.B., Singer, B.S., Meyers, S.R., Siewert, S.E., Walaszczyk, I., Condon, D.J., Jicha, B.R., Obradovich, J.D., Sawyer, D.A., 2014. Integrating  $^{40}\text{Ar}/^{39}\text{Ar}$ , U-Pb, and astronomical clocks in the Cretaceous Niobrara Formation, Western Interior Basin, USA. *Geol. Soc. Am. Bull.* 126 (7–8), 956. <http://dx.doi.org/10.1130/b30929.1>.
- Schmitz, B., Pujalte, V., Molina, E., Monechi, S., Orue-Etxebarria, X., Speijer, R.P., Alegret, L., Apellaniz, E., Arenillas, I., Aubry, M.-P., Baceta, J.-I., Berggren, W.A., Bernaola, G., Caballero, F., Clemmensen, A., Dinarès-Turell, J., Dupuis, C., Heilmann-Clausen, C., Hilario Orus, A., Knox, R., Martin-Rubio, M., Ortiz, S., Payros, A., Petrizzi, M.R., von Salis, K., Sprong, J., Steurbaut, E., Thomsen, E., 2011. *The Global Stratotype Sections and Points for the bases of the Selandian (Middle Paleocene) and Thanetian (Upper Paleocene) stages at Zumaia, Spain*.  *Episodes* 34, 220–243.
- Schulz, M., Mudelsee, M., 2002. REDFIT: estimating red-noise spectra directly from unevenly spaced paleoclimatic time series. *Comput. Geosci.* 28, 421–426. [http://dx.doi.org/10.1016/S0098-3004\(01\)00044-9](http://dx.doi.org/10.1016/S0098-3004(01)00044-9).
- ten Kate, W.G.H.Z., Sprenger, A., 1993. Orbital cyclicities above and below the Cretaceous/Paleogene boundary at Zumaya (N Spain), Agost and Relleu (SE Spain). *Sediment. Geol.* 87, 69–101. [http://dx.doi.org/10.1016/0037-0738\(93\)90037-6](http://dx.doi.org/10.1016/0037-0738(93)90037-6).
- Torrence, C., Compo, G.P., 1998. A practical guide to wavelet analysis. *Bull. Am. Meteorol. Soc.* 79, 61–78. [http://dx.doi.org/10.1175/1520-0477\(1998\)079<0061:APGTWA>2.0.CO;2](http://dx.doi.org/10.1175/1520-0477(1998)079<0061:APGTWA>2.0.CO;2).
- Varadi, F., Runnegar, B., Ghil, M., 2003. Successive refinements in long-term integrations of planetary orbits. *Astrophys. J.* 592, 620–630. <http://dx.doi.org/10.1086/375560>.
- Westerhold, T., Röhl, U., Raffi, I., Fornaciari, E., Monechi, S., Reale, V., Bowles, J., Evans, H.F., 2008. Astronomical calibration of the Paleocene time. *Palaeogeogr. Palaeoclimatol. Palaeoecol.* 257, 377–403. <http://dx.doi.org/10.1016/j.palaeo.2007.09.016>.
- Westerhold, T., Röhl, U., Donner, B., McCarren, H.K., Zachos, J.C., 2011. A complete high-resolution Paleocene benthic stable isotope record for the central Pacific (ODP Site 1209). *Paleoceanography* 26. <http://dx.doi.org/10.1029/2010pa002092>.
- Westerhold, T., Röhl, U., Laskar, J., 2012. Time scale controversy: accurate orbital calibration of the Early Paleogene. *Geochem. Geophys. Geosyst.* 13. <http://dx.doi.org/10.1029/2012gc004096>.
- Wilkens, R.H., Niklis, N., Frazer, M., 2009. Data report: digital core images as data: an example from IODP Expedition 303. In: Channell, J.E.T., Kanamatsu, T., Sato, T., Stein, R., Alvarez Zarikian, C.A., Malone, M.J., the Expedition 303/306 Scientists (Eds.), *Proc. IODP, vol. 303/306. Integrated Ocean Drilling Program Management International, Inc., College Station, TX*.
- Zachos, J.C., Kroon, D., Blum, P., et al., 2004. In: *Proc. ODP, Init. Repts., vol. 208. Ocean Drilling Program, College Station, TX*.